The C_3-bending vibrational levels of the C_3–Kr and C_3–Xe van der Waals complexes studied by their $\tilde{A} - \tilde{X}$ electronic transitions and by *ab initio* calculations

Jun-Mei Chao,[1] Keng Seng Tham,[1] Guiqiu Zhang,[1,a] Anthony J. Merer,[1,b]
Yen-Chu Hsu,[1,c] and Wei-Ping Hu[2]
[1]*Institute of Atomic and Molecular Sciences, Academia Sinica, P. O. Box 23-166, Taipei 10617, Taiwan*
[2]*Department of Chemistry and Biochemistry, National Chung-Cheng University, Min-Hsiung, Chia-Yi 62102, Taiwan*

Fluorescence excitation spectra and wavelength-resolved emission spectra of the C_3–Kr and C_3–Xe van der Waals (vdW) complexes have been recorded near the $2^{2-}{}_0$, $2^{2+}{}_0$, $2^{4-}{}_0$, and $1^1{}_0$ bands of the $\tilde{A}\,^1\Pi_u - \tilde{X}\,^1\Sigma_g^+$ system of the C_3 molecule. In the excitation spectra, the spectral features of the two complexes are red-shifted relative to those of free C_3 by 21.9–38.2 and 34.3–36.1 cm^{-1}, respectively. The emission spectra from the $\tilde{A}$ state of the Kr complex consist of progressions in the two C_3-bending vibrations (ν_2, ν_4), the vdW stretching (ν_3), and bending vibrations (ν_6), suggesting that the equilibrium geometry in the $\tilde{X}$ state is nonlinear. As in the Ar complex [Zhang *et al.*, J. Chem. Phys. **120**, 3189 (2004)], the C_3-bending vibrational levels of the Kr complex shift progressively to lower energy with respect to those of free C_3 as the bending quantum number increases. Their vibrational structures could be modeled as perturbed harmonic oscillators, with the dipole-induced dipole terms of the Ar and Kr complexes scaled roughly by the polarizabilities of the Ar and Kr atoms. Emission spectra of the Xe complex, excited near the $\tilde{A}$, 2^{2-} level of free C_3, consist only of progressions in even quanta of the C_3-bending and vdW modes, implying that the geometry in the higher vibrational levels ($\upsilon_{\text{bend}} \geq 4$, $E_{\text{vib}} \geq 328$ cm^{-1}) of the $\tilde{X}$ state is (vibrationally averaged) linear. In this structure the Xe atom bonds to one of the terminal carbons nearly along the inertial *a*-axis of bent C_3. Our *ab initio* calculations of the Xe complex at the level of CCSD(T)/aug-cc-pVTZ (C) and aug-cc-pVTZ-PP (Xe) predict that its equilibrium geometry is T-shaped (as in the Ar and Kr complexes), and also support the assignment of a stable linear isomer when the amplitude of the C_3 bending vibration is large ($\upsilon_4 \geq 4$). © 2011 American Institute of Physics. [doi:10.1063/1.3506635]

I. INTRODUCTION

The van der Waals (vdW) complexes of rare-gas (Rg) atoms with various molecules have been studied extensively. Where the complexes are T-shaped, it has been found that as the rare gas atom varies from Ne to Xe, the vdW bond lengths and bond angles change only slightly. This happens partly because the increasing atomic radius of the Rg atom compensates for some of its increasing polarizability,[1] and partly because the vdW bond length is greater than the sum of the atomic radii.[2] Although the vdW bond lengths of the Rg–CO complexes change very little as the atomic number of the Rg atom increases, the bond angle becomes more nearly 90°.[2] The anisotropy of the angular potential for T-shaped complexes is expected to be greater for Xe than for other Rg atoms. Since the atomic radius of Xe is comparatively large and the binding energy is greatest for Xe complexes, a small angle deviation from the equilibrium geometry of a Xe complex will cause its energy to rise rapidly. Similar phenom-

ena have been reported for non-T-shaped complexes, such as Xe–H_2 (Ref. 3) and Xe–CH_4.[4]

By contrast, certain rare gas complexes exist in isomeric forms. Isomers occur for He and Ne complexes because of their weak vdW bonds and small angular anisotropy. The vibrational amplitudes are often large in such complexes, which makes their geometry determinations difficult.[5] As for complexes with heavier rare gas atoms, both linear (L-) and T-shaped isomers have been reported for Ar–I_2 (Refs. 6 and 7) and Ar–Br_2.[8,9] Although the two isomers of Ar–Br_2 are energetically nearly degenerate, the lines in the optical spectra of the T-shaped isomer are sharp[8] while those of the linear isomer are diffuse[9] as a result of a bound-to-free transition. The spectroscopic characterizations of the isomers of other Rg-molecule complexes could be useful in understanding matrix isolation spectroscopy.

Wavelength-resolved emission spectra from the $\tilde{A}$ state of the C_3–Ar complex have previously allowed us to map the C_3-bending vibrational levels of its ground electronic state.[10] The results showed that the level structure can be modeled as a harmonic oscillator perturbed by a dipole-induced dipole interaction potential.[10] As the C_3 molecule bends away from its linear configuration its dipole moment increases, which has the effect of stabilizing the Ar complex, and lowering its levels

relative to those of free C_3 by as much as 82 cm^{-1} at $\upsilon_b = 10$. The observed C_3-bending vibrational levels of the Ar complex were assigned as the progression $\upsilon_{2, \text{in-plane}} = 1$, $\upsilon_{4, \text{out-of-plane}} = \upsilon_b - 1$, ($\upsilon_b = \upsilon_2 + \upsilon_4 \geq 2$), consistent with the near-T-shaped equilibrium geometry predicted by our *ab initio* calculation. No linear isomer was found. Wavelength-resolved emission spectra of the Ar complex therefore allowed us to study higher bending levels of the vdW complex, ($\upsilon_b \geq 4$), which would not be observable in microwave and infrared experiments, where only the lowest levels can be seen.

One of the aims of the present work is to test whether our perturbed harmonic oscillator (PHO) model for the Ar complex can be extended to the Kr and Xe complexes. The results provide experimental evidence that the geometries of both the $\tilde{X}$ and $\tilde{A}$ states of the Kr complex are T-shaped (like those of the Ar complex), and that our PHO model works well for the C_3-bending vibrational levels of its ground electronic state. To our surprise, wavelength-resolved fluorescence spectra of the Xe complex indicate the existence of an L-isomer at $\upsilon_b \geq 4$. The potential energy surfaces of the Ar and Xe complexes calculated in our previous work[10] and this work give the relative stabilities of the L-isomers of these two complexes.

II. EXPERIMENTAL DETAILS

Two different types of nozzle were used in this work: a home-made slit nozzle (2 mm $\times$ 50 μm) and a circular nozzle with a 500 μm diameter. The slit nozzle was used for collecting emissions from weak vdW transitions and for reducing the Doppler width of the excitation spectra. The gas mixture used for generating the Kr and Xe complexes was 0.03%–0.06% of allene, 4% of Kr or Xe, with a balance of 50:50 He:Ne gas mixture. To eliminate the possibility of interference by the Ne complex, which might be formed at this high Ne concentration, some experiments with the Xe complex were carried out using pure He instead of the 50:50 He:Ne mixture. Lower concentrations (0.03%) of allene were used when it was necessary to reduce the internal energy of the vdW complex. The backing pressure was typically about 5.3 atm.

The gas mixture was photolysed by radiation from an ArF (193 nm) excimer laser (Lambda Physik, LPX 110i), aligned so as to intersect the supersonic molecular beam near the tip of the nozzle orifice. Since it requires two 193 nm photons to dissociate allene to produce C_3, the focusing has to be carried out carefully so as to minimize three-photon dissociation processes. Three-photon processes give translationally and rotationally hot C_3 molecules, which lower the yield of the C_3–Rg vdW complex.

The bands of the C_3–Rg vdW complexes accompanying the $\tilde{A}\,^1\Pi_u - \tilde{X}\,^1\Sigma_g^+$ system of C_3 were probed by laser-induced fluorescence (LIF) and wavelength-resolved emission methods. To obtain fluorescence excitation spectra of the Kr and Xe complexes, a tunable dye laser (Lumonics Inc. HD 500) was scanned in the range of 388–405 nm. The LIF spectra were calibrated against simultaneously recorded optogalvanic spectra of an Fe–Ne hollow cathode lamp.[11] The relative frequencies reported here are accurate to at least ± 0.1 cm^{-1}; however, the absolute frequencies appear to be good only to ± 0.5 cm^{-1}, comparing our measurements of the C_3 bands with those reported in Refs. 12–14.

In the wavelength-resolved emission experiments, the fluorescence was dispersed by a 0.3-m-monochromator (Jobin-Yvon HR 30) with a 2400 lines/mm grating. The slit width was set to 40–100 μm, depending upon the fluorescence intensity of the band under study; the spectral resolution of the emission therefore ranges from 8.5 to 20 cm^{-1}. Spectral calibration was carried out using emission lines from an Fe–Ne hollow cathode lamp.[11] The absolute frequencies of the C_3 emission lines agree to ± 2 cm^{-1} with the stimulated emission pumping measurements of Northrup and Sears.[15] More details of the experimental conditions can be found elsewhere.[10]

III. FLUORESCENCE EXCITATION SPECTRA OF THE C_3–Kr AND C_3–Xe vdW COMPLEXES

Fluorescence excitation spectra of the C_3–Kr and C_3–Xe complexes have been recorded near the (0,0), $2^{2-}{}_0$, $2^{2+}{}_0$, $2^{4-}{}_0$, and $1^1{}_0$ bands of the $\tilde{A}\,^1\Pi_u - \tilde{X}\,^1\Sigma_g^+$ system of the C_3 monomer. Figure 1 shows the excitation spectra of the Kr complex near these five bands. The R(0) lines of the various C_3 bands in Fig. 1 have been aligned vertically in the panels. The excitation spectra of the Kr complex are very similar to those of the Ar complex;[10] for instance, (i) no vdW band is observed near the (0,0) band of C_3, (ii) vdW bands were observed both to the red (low-frequency side) and blue

FIG. 1. The fluorescence excitation spectra of the C_3–Kr complex recorded near the (0,0), $2^{2-}{}_0$, $2^{2+}{}_0$, $2^{4-}{}_0$, and $1^1{}_1$ bands of the Comet system of C_3 under supersonic beam conditions. The spectral features marked with arrows were assigned to the Kr complex. The R(0) lines of the C_3 bands in each panel have been lined up vertically. The low-frequency side of the excitation spectrum recorded near the (0,0) band was shifted upwards and its intensity was enhanced by a factor of 5 to show that no Kr complex was observed.

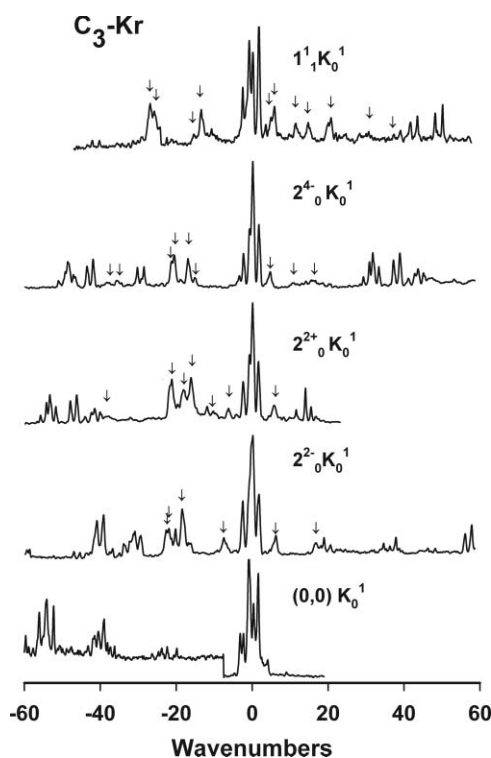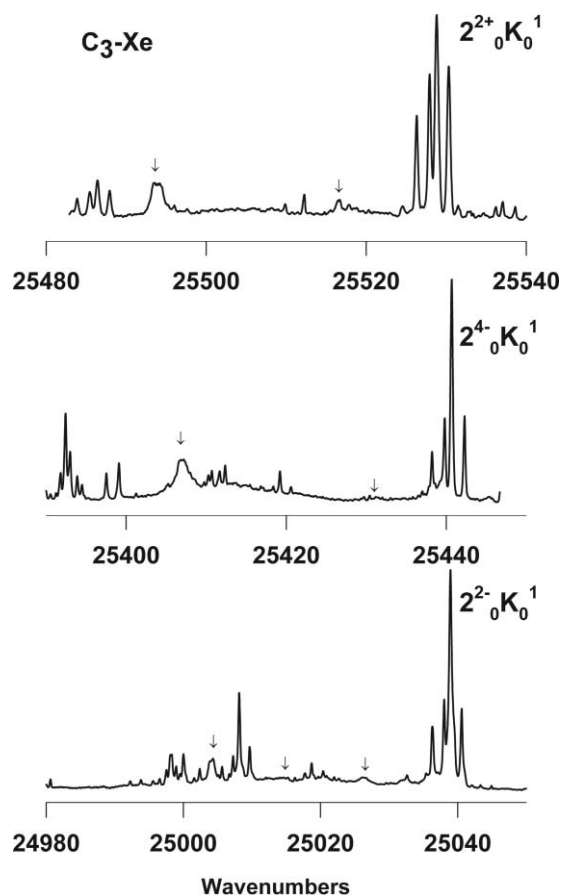074313-3 C_3-bending levels of C_3–Kr and C_3–Xe

J. Chem. Phys. **134**, 074313 (2011)

FIG. 2. The fluorescence excitation spectra of the C_3–Xe complex recorded near the $2^{2-}{}_0$, $2^{2+}{}_0$, and $2^{4-}{}_0$ bands of the Comet system of C_3 under supersonic beam conditions. Spectral features marked with arrows were assigned to the Xe complex.

TABLE I. Largest red-shifts (cm^{-1}) observed in the C_3–Ar, C_3–Kr, and C_3–Xe van der Waals complexes from the R(0) lines of the free C_3 transitions.

	$2^{2-}{}_0$	$2^{2+}{}_0$	$2^{4-}{}_0$
Ar	14.2	31.1	35.5
Kr	21.9	38.1	38.1
Xe	34.3	34.9	33.8

mixes the characters of the 2^{2+} and 2^{4-} levels quite strongly and also mixes them with higher bending levels. Since higher bending levels of C_3 (Ã) are expected to have larger dipole moments, the vdW bond in C_3 (Ã, 2^{2+} or 2^{4-})–Rg should be stronger than that in C_3 (Ã, 2^{2-})–Rg. This could explain the larger red-shifts observed in these two bands of the Ar and Kr complexes. However, the red-shifts of these three bands in the Xe complex seem to have reached a limiting value. Perhaps this limit arises from poorer Franck–Condon factors which prevent us from observing the full vdW progressions near the $2^{2+}{}_0$ and $2^{4-}{}_0$ bands of C_3.

(high-frequency side) of the transitions to vibrationally excited C_3(Ã), (iii) vdW bands to the red of the C_3 transitions are much more intense than those to the blue, (iv) the most intense vdW band is a doublet, and (v) the largest vdW shifts were observed near the $2^{2+}{}_0$ and $2^{4-}{}_0$ bands of the C_3 system.

For the Xe complex, again no band was found near the (0, 0) band of the C_3 system. Since there are strong singlet–triplet perturbations in the zero-point level of the Ã state,[12, 16] it is quite probable that the zero-point level of the Ã state of the C_3–Rg complex undergoes fast vibrational predissociation from the triplet manifolds through the singlet–triplet mixed doorway states.[10] The excitation spectra of the Xe complex near the $2^{2-}{}_0$, $2^{2+}{}_0$, and $2^{4-}{}_0$ bands of C_3 (shown in Fig. 2) have fewer progressions than those of the Ar and Kr complexes and bands were only observed to the red side of the C_3 bands. Most of the Xe complex bands are too broad to show any evidence of doublet structure.

Table I lists the largest frequency shifts observed for the Ar, Kr, and Xe vdW complexes near the $2^{2-}{}_0$, $2^{2+}{}_0$, and $2^{4-}{}_0$ bands of free C_3. These represent the amounts by which the C_3-bending levels of the complexes are lowered relative to those of free C_3. Near the $2^{2-}{}_0$ band of C_3, the observed vdW red-shifts simply follow the trend of the increasing polarizabilities of the Ar, Kr, and Xe atoms; this suggests that the Ã, 2^{2-} level of C_3 is only slightly perturbed by the nearby Rg atom. The orbital angular momentum of the Ã state[17] of C_3

FIG. 3. Top figure: Excitation spectrum of C_3–Kr near the $2^{2-}{}_0$ band of free C_3. Below are traces of the wavelength-resolved emission spectra obtained by exciting the blended R(0) and Q(2) lines of C_3 and by exciting the Kr complex at the vdW bands labeled A–D, respectively.

Downloaded 21 Feb 2011 to 163.28.96.9. Redistribution subject to AIP license or copyright; see http://jcp.aip.org/about/rights_and_permissions

FIG. 4. Top figure: Excitation spectrum of C_3–Kr near the 2^4_0 band of free C_3. Below are traces of the wavelength-resolved emission spectra obtained by exciting the blended R(0) and Q(2) lines of C_3 and by exciting the Kr complex at the vdW bands labeled E–G, respectively.
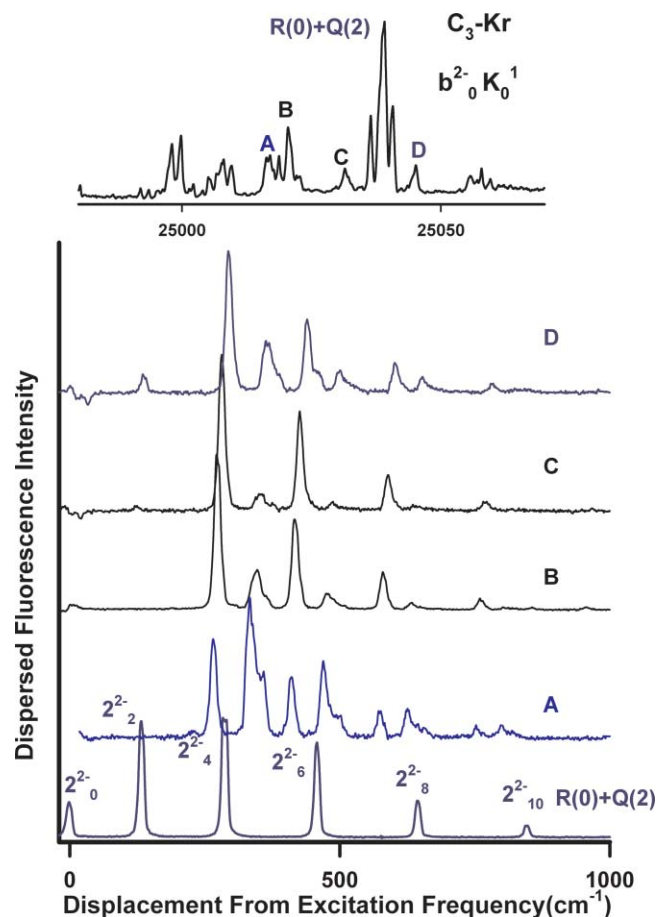

FIG. 5. Top figure: Excitation spectrum of C_3–Kr near the 1^1_0 band of free C_3. Below are traces of the wavelength-resolved emission spectra obtained by exciting the blended R(0) and Q(2) lines of C_3 and by exciting the Kr complex at the vdW bands labeled H–K, respectively.
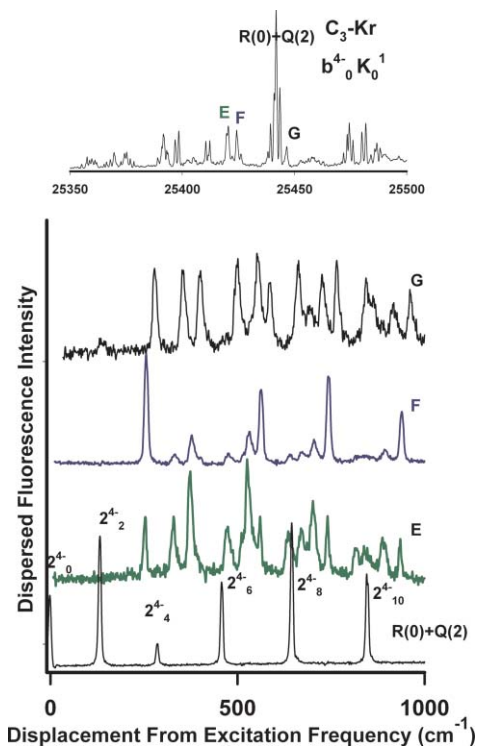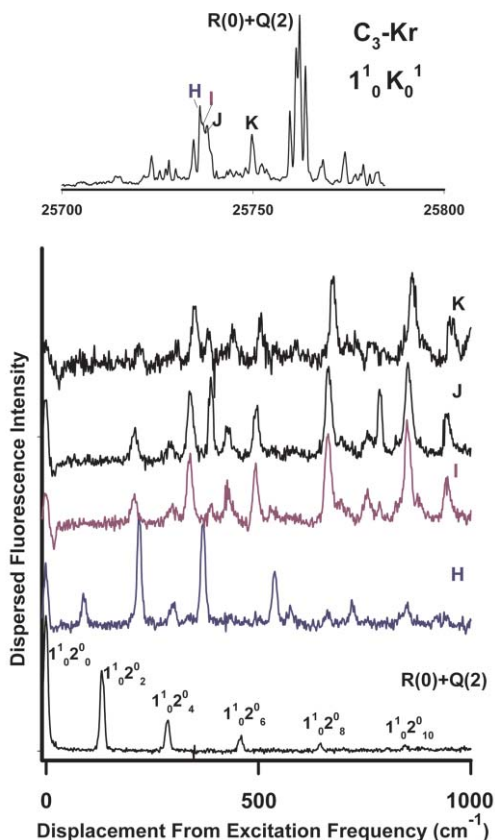
IV. WAVELENGTH-RESOLVED EMISSION SPECTRA OF THE C_3–Kr COMPLEX

Figures 3–5 illustrate wavelength-resolved emission spectra obtained by exciting free C_3 or its Kr complex, at or near the 2^{2-}_0, 2^{4-}_0, and 1^1_0 bands of C_3. Each figure is in three parts. The top trace is the excitation spectrum, showing the bands of the Kr complex superimposed on the bands of free C_3. Letters indicate the bands of the complex from which wavelength-resolved emission spectra (shown in the middle part of the figure) were recorded. At the bottom of the figure is the emission spectrum given by the C_3 band itself. All the bands examined arise from the ground vibrational level of C_3 or the Kr complex, so that the energies of the lower levels of the various emission features can be obtained directly, by subtracting the observed emission frequency from the excitation frequency. Fourteen bands of the Kr complex, observed near the 2^{2-}_0, 2^{2+}_0, 2^{4-}_0, and 1^1_0 bands of C_3, have been studied by this dispersed fluorescence (DF) method. No emission was observed from free C_3 itself, indicating that the Ã-state complex of this study is bound.

Some excitation bands of the Kr complex are much broader than the spectral resolution (~ 0.25 cm^{-1}) of our pulsed dye laser. For these broad vdW bands, such as those at 25 017 and 25 737 cm^{-1}, we recorded more than one DF spectrum, setting the excitation laser to different parts of the broad profile. As shown in Fig. 5, where three close-lying excitation frequencies (25 736.1, 25 737.0, and 25 738.0 cm^{-1}) were chosen, it is seen that the emission spectrum obtained by exciting the Kr complex at 25 736.1 cm^{-1} (labeled as H) is quite different from the other two (labeled as I and J), suggesting that the broad feature is an unresolved blend of two, or possibly more, vdW bands. Table II lists the observed vibrational levels of the Kr complex up to 1000 cm^{-1} above its ground vibrational level. In this region only C_3-bending, vdW stretching, and vdW bending vibrations are expected, since the stretching vibrations of free C_3 lie above this energy. Following Ref. 10, we number the vibrational modes of the Kr complex assuming C_{2v} symmetry: ν_1 and ν_5 are the symmetric and antisymmetric C–C stretching vibrations, ν_2 (a_1) and ν_4 (b_1) are the in-plane and out-of-plane C_3-bending vibrations and ν_3 (a_1) and ν_6 (b_2) are the vdW stretching and bending vibrations.

Of all the C_3–Kr emission spectra, those from the vdW levels of the Ã, b^{2-} state (b refers to the bending of the C_3 portion of the complex) shown in Fig. 3 are the simplest, with almost no activity in the ground state vdW modes. In this figure both even and odd quanta of the C_3-bending vibration can be seen, suggesting that both the upper and lower states of the Kr complex are nonlinear. A Franck–Condon node occurs at the expected position of the X̃, $\upsilon_2'' + \upsilon_4'' = 2$ levels (near $\nu_{laser} - 140$ cm^{-1}). A similar Franck–Condon pattern is found in the Ar complex,[10] though the latter has fewer levels with $\upsilon_b'' = $ odd. In contrast, it is interesting to note that the $\upsilon_2'' + \upsilon_4'' = 2$ levels are observed in the Ne complex.[18]

Following the same procedure as described in Sec. VI of Ref. 10, the PHO model has been used to fit the observed C_3-bending vibrational levels of the ground electronic state of the Kr complex. A satisfactory fit could be obtained if the

TABLE II. The energies and vibrational assignments of the lower levels observed from the emission of seventeen C$_3$–Kr upper levels at 25016.6,[a] 25017.1, 25020.6,[b] 25031.8,[c] 25045.4,[d] 25507.9, 25511.1, 25513.0, 25420.6,[e] 25424.3,[f] 25446.6,[g] 25734.5,[h] 25736.1,[i] 25737.0, 25738.0,[j] 25749.7,[k] and 25768.4 cm^{-1}.

Vibrational assignment[l]	$v_b' = 2^-$					$v_b' = 2^+$			$v_b' = 4^-$			$v_1' = 1$					
	25016.6	25017.2	25020.6	25031.8	25045.4	25507.9	25511.1	25513.0	25420.6	25424.3	25446.6	25734.5	25736.1	25737.0	25738.0	25749.7	25768.4
b_0												0.0	0.0				
$b_0 3_1$	50					36.7											
$b_0 3_1 6_2$																	
b_1								63									
$b_1 6_3$												89	87.3				
$2_1 6_1$				122													
$2_1 6_3$					135						138						
?										141							
$2_1 4_2 6_1$														209	210		
$2_2 4_1$	229	225.5										219	219.2			218.4	
$2_2 4_1 6_1$																	230
$2_2 4_1 6_3$																	246
$2_2 3_1 4_1$									253.2	256.2							251(b)[m]
$2_1 4_3$	268	265.6	273	281													
$2_1 4_3 6_1$											279						
$2_1 4_3 6_2$																	
$2_2 4_2$	296.4				293							294		298	292		
$2_1 3_1 4_3$													302.9			305.3	313
$2_2 4_2 6_2$						289	293	288									
$2_1 4_4$	334	333.6	336			340.5	344		330	332				340	338		
$2_1 4_4 6_2$		348.4	347	354.7				347	340							349.5	
$2_1 4_4 6_3$								359									
$2_2 4_3$	360	358.4	363	363							356						
$2_1 3_1 4_4$				375	370				373.6			369	370.4				364
$2_1 3_1 4_4 6_1$								378		378							
$2_3 4_1$					387									390	388	380	
$2_3 4_1 6_2$									392	401	402						

TABLE II. (*Continued.*)

Vibrational assignment[1]	$v_b' = 2^-$					$v_b' = 2^+$			$v_b' = 4^-$			$v_1' = 1$					
	25016.6	25017.2	25020.6	25031.8	25045.4	25507.9	25511.1	25513.0	25420.6	25424.3	25446.6	25734.5	25736.1	25737.0	25738.0	25749.7	25768.4
$2_1 4_5$	412	410.4	416.5			417	416.7	418.5									
$2_1 4_5 6_2$				426										427	427.9		
$2_1 4_5 6_3$					439		434.6	437.2					435.1			438.3	
$2_2 4_4$						431											
$2_2 4_4 6_2$																	456
$2_2 4_4 6_3$					453	464.1	462.6	461.8									
$2_1 4_6$	470	469.1					474.1		473	475							
$2_1 4_6 6_1$		481.3	477														
$2_1 4_6 6_2$			490	486					487.7								
$2_2 4_5$	495	494.6						493			493		493.7	494.8			
$2_2 4_5 6_1$											500				498		
$2_1 3_1 4_6$					501				511.7							506.4	
$2_2 4_5 6_2$								519.0		517	517						519
$2_2 4_5 6_3$									526.8			526.3		527			
$2_2 4_5 6_4$									541.3								
$2_2 3_1 4_5$										532							
$2_2 3_1 4_5 6_1$											540	538.4	540				
$2_2 3_1 4_5 6_2$											553						
$2_2 3_1 4_5 6_4$						564.2	562.1		560	563							
$2_1 4_7$	573.5	574.7	579.2					572			569	573.4					
$2_1 4_7 6_1$							578.1					582.5					
$2_1 4_7 6_2$				589							587					586.0	588.7
$2_1 4_7 6_3$																	
$2_2 4_6$					602.4	596.4		601.1									600
$2_1 3_1 4_7$						611.2	612.4	616.2									
$2_2 4_6 6_2$						616.4	622.7										
$2_1 4_8$	625.9	625.3	633.5	637.3		627.5	637.3	634	636								
$2_1 4_8 6_1$	647.2	645.6				649.6				639							

074313-7 C_3-bending levels of C_3–Kr and C_3–Xe J. Chem. Phys. **134**, 074313 (2011)

TABLE II. (*Continued.*)

Vibrational assignment[a]	$v_b' = 2^-$					$v_b' = 2^+$			$v_b' = 4^-$			$v_1' = 1$					
	25016.6	25017.2	25020.6	25031.8	25045.4	25507.9	25511.1	25513.0	25420.6	25424.3	25446.6	25734.5	25736.1	25737.0	25738.0	25749.7	25768.4
	660.5	657.4			657.5		655	656				655.3					
									671	670	664		663.2	664	666		
											676					677.1	
																	692.5
									701.2	704	694			694	694		706
												717.2		710.8		708.7	714
						723	727.7				726.7	724.5	724.1			726.7	722
						733.5		732.0	740.4	743							
$2_1 4_9$	755.5	752.3				757.7	759	761.9						757	756		
$2_1 4_9 6_1$			760								766					766	
$2_1 4_9 6_2$				772													
$2_1 4_9 6_3$																	
$2_2 4_8$	785.2				783	774.5	780.6	780.2					787.5	785	785		783
$2_1 3_1 4_9$								789									
$2_2 4_8 6_1$							798.9	793								797	
$2_1 3_1 4_9 6_1$																	
$2_1 4_{10}$	799.6	799.6	802			805.3			817.6						824		820
	822.3	819.5															
$2_1 3_1 4_{10}$	843.6		857		837	833.2	836.8	836.3	838	839	837	850	846	849	852	862	852
	886					858.5	859.4	856.5	887	862.1	844.5			874		886	878
									887	887	852.1						
											861.5						
											884.3						

TABLE II. (*Continued.*)

Vibrational assignment[l]	$v_b' = 2^-$					$v_b' = 2^+$			$v_b' = 4^-$			$v_1' = 1$					
	25016.6	25017.2	25020.6	25031.8	25045.4	25507.9	25511.1	25513.0	25420.6	25424.3	25446.6	25734.5	25736.1	25737.0	25738.0	25749.7	25768.4
								890.6	894	893							895
						907.9	913.2	912.6			911.7						902
													922.6				
						930.1	939		934	939							
								945.1					943.1	944	945		
			958				959.9									955	
						970.7											971
							975	975.6									
																	983
																	1016.5
																	1032.8

[a]Band A of Fig. 3.
[b]Band B of Fig. 3.
[c]Band C of Fig. 3.
[d]Band D of Fig. 3.
[e]Band E of Fig. 4.
[f]Band F of Fig. 4.
[g]Band G of Fig. 4.
[h]Band H of Fig. 5.
[i]Band I of Fig. 5.
[j]Band J of Fig. 5.
[k]Band K of Fig. 5.
[l]v_1 and v_5 are the symmetric and antisymmetric C–C stretching vibrations, v_2 and v_4 are the in-plane and out-of-plane C_3-bending vibrations, and v_3 and v_6 are the vdW stretching and bending vibrations.
[m]Broad line.

TABLE III. The observed and calculated C$_3$-bending vibrational levels of C$_3$–Kr using the PHO model. All parameters and the standard deviation of the fit are in units of cm^{-1}.

υ_b	(υ_2, υ_4)	obs	obs-cal
4	(1,3)	268.0	7.1
	(2,2)	296.4	9.7
5	(1,4)	334.0	1.7
	(2,3)	360.0	1.5
6	(1,5)	412.0	4.0
	(2,4)	438.0	3.2
7	(1,6)	470.0	− 17.8
	(2,5)	495.0	− 20.2
8	(1,7)	574.0	2.6
	(2,6)	600.0	0.4
9	(1,8)	626.0	–
10	(1,9)	756.0	6.6
	(2,8)	785.0	5.9
	σ^a		9.1
	V_1		0.0(fixed)
	$|V_2|$		6.3 ± 0.3

$\upsilon_2 = 111.2(72)$, $\upsilon_4 = 40.2(33)$, $x_{22} = -10.0$(fixed), $x_{24} = 5.0(15)$, $x_{44} = 3.07(42)$, $\sigma = 7.1$ cm^{-1}

^{a}One standard deviation of the error of the fit.

observed levels of each υ_b'' manifold were assigned as (υ_2'' = 1, $\upsilon_4'' = \upsilon_b'' - 1$) and ($\upsilon_2'' = 2$, $\upsilon_4'' = \upsilon_b'' - 2$). The results are listed in Table III. The observed C$_3$-bending vibrational levels with $\upsilon_b'' = 9$ have not been included in the fit because they give residuals of more than three standard deviations of the fit. (This was the case also with the Ar complex.) The poor fit for the $\upsilon_b'' = 9$ level in both the complexes possibly results from the lack of precise measurements for the odd υ_b'' levels (≥ 11) of free C$_3$,[15,19,20] which are the basis states in the PHO model.

The dipole-induced dipole interaction strength of the Kr complex obtained from this fit is $|V_2| = 6.3$ (3) cm^{-1}, which is about 1.3 times that of the Ar complex,[10] where $|V_2|$ = 4.8 (4) cm^{-1}. The increase in $|V_2|$ can be explained by the larger polarizability of Kr compared to Ar. Given the polarizabilities of the Kr and Ar atoms (2.484 × 10^{-24} and 1.641 × 10^{-24} cm^3, respectively)[21] and the *ab initio* calculated bond length of C$_3$–Ar (3.9 Å),[10] the values of V$_2$ allow the bond length of the C$_3$–Kr complex to be estimated as 4.0 Å, using the formula for dipole-induced dipole interaction.[22] The fairly small change in the vdW bond length from the Ar complex to the Kr complex, which is consistent with previous reports on CO and NO,[1,2] is supported by our *ab initio* calculations. Calculations[23] of the Kr complex could only be made with smaller basis sets [aug-cc-pVTZ (C) (Refs. 24 and 25) and aug-cc-pVTZ-pp (Kr) (Ref. 26)] than those used for the Ar complex (cc-pVQZ). It is expected that the vdW bond length predicted by the aug-cc-pVTZ basis set will be shorter by 0.1 Å than that predicted by cc-pVQZ. The *ab initio* calculated vdW bond length of the Kr complex is 3.9 Å. Applying the same corrections for the different basis sets as those used for the C$_3$–Ar complex, the bond length changes to 4.0 Å, which (possibly coinciden-

tally) is the same as that given by the dipole-induced dipole model.

The C$_3$-bending levels have also been fitted with a two-dimensional anharmonic oscillator model, giving $\upsilon_2 = 111.2(72)$ and $\upsilon_4 = 40.2(33)$ cm^{-1} (see Table III). The large anharmonicities obtained from the fit result from the large–small staggering of the level spacings of the υ_4 mode, which possibly indicate that the vdW motion has a double minimum vibrational potential. Unfortunately, the PHO model does not take into account the coupling of υ_4 with the vdW bend and vdW stretch. From Table II, three other vibrational intervals, 27(2), 37(2), and 8(2) cm^{-1}, can be identified. The 27(2) cm^{-1} interval is assigned as the separation of different components of a υ_b-polyad, such as ($\upsilon_2 = 1$, $\upsilon_4 = \upsilon_b - 1$) and ($\upsilon_2 = 2$, $\upsilon_4 = \upsilon_b - 2$), where $\upsilon_2 + \upsilon_4 = \upsilon_b$. The 37(2) and 8(2) cm^{-1} intervals are assigned to the ν_3 and ν_6 vibrations of the Kr complex, respectively. It is possible to estimate the vdW stretching frequency, ν_3, by solving a one-dimensional Schrödinger equation using a perturbation method; the vdW stretching potential was first obtained from *ab initio* calculations[23] at the level of CCSD(T)/aug-cc-pVTZ(C) and aug-cc-pVTZ-pp (Kr), and the data were then fitted to a Morse-like function,

$$V(R) = V_0 + a \exp(-bR) + c \exp(-dR). \qquad (1)$$

Taking $\rho(\angle C–C–C) = 170°$ and ϕ (the in-plane angle, at the center of mass of the C$_3$ molecule, between its a-axis and the Xe atom) = 90°, the ν_3 frequency is given as 38.6 cm^{-1} and the anharmonicity constant x_{33} as −1.355 cm^{-1}. A small frequency interval of 3–5 cm^{-1}, found in the emission spectra, could not be assigned. As a result, some of the levels, particularly those with $\upsilon_b'' = 9$, have not been assigned in Table II.

V. WAVELENGTH-RESOLVED EMISSION SPECTRA OF THE C$_3$–Xe COMPLEX

As is the case with the other C$_3$–Rg vdW molecules, no Xe-complex features were observed near the (0,0) band of the $\tilde{A}-\tilde{X}$ system of C$_3$. Table IV lists the ground state energy levels given by the wavelength-resolved emission spectra from seven C$_3$–Xe bands near the $2^-{}_0$, $2^+{}_0$, and $2^4{}_0$ bands of C$_3$. Representative spectra are illustrated in Figs. 6 and 7. Because the fluorescence intensity from the Xe-complex is quite weak, the slit width of the monochromator had to be widened to 100 μm in order to record emission spectra from bands B and C in Fig. 6; the spectral resolution of the emission from these two bands is therefore reduced to about 20 cm^{-1}. Band A in Fig. 6 and bands D and E in Fig. 7 are stronger, so that their emission spectra could be recorded with slightly better resolution, 12 cm^{-1}. As Fig. 7 shows, the emission features with displacements, $\nu_{laser} - \nu = 600-1000$ cm^{-1} show signs of diffuseness. It is not clear whether this is caused by predissociation or spectral congestion. However the emission spectra contain no bands that can be assigned to C$_3$ itself, suggesting that electronically excited C$_3$ is not formed when these bands of the complex are excited. (This is the case also in the emission spectra of the Ar and Kr complexes.[10]) We
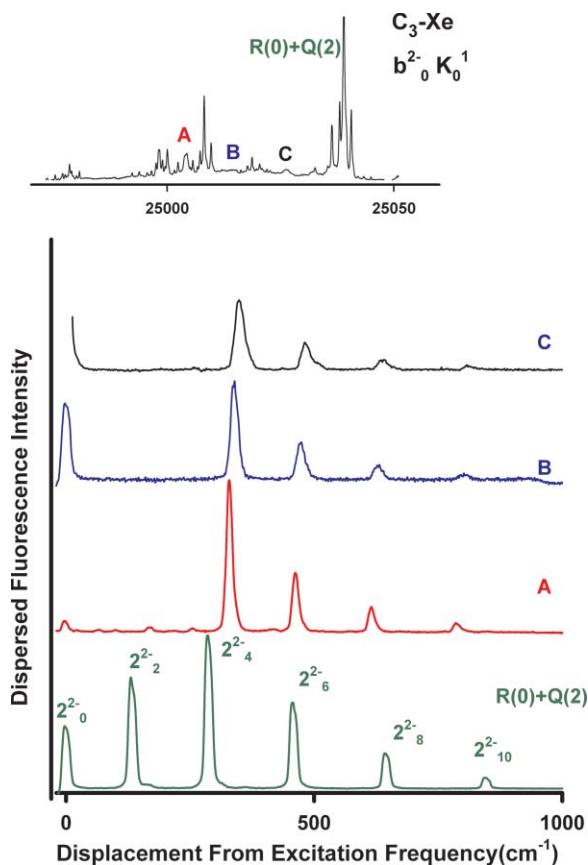
FIG. 6. Top figure: excitation spectrum of the Xe complex near the 2^{2-}_0 band of free C_3. Below are traces of the wavelength resolved emission spectra obtained by exciting the blended R(0) and Q(2) lines of C_3 and by exciting the Xe complex at the vdW bands labeled A–C, respectively.
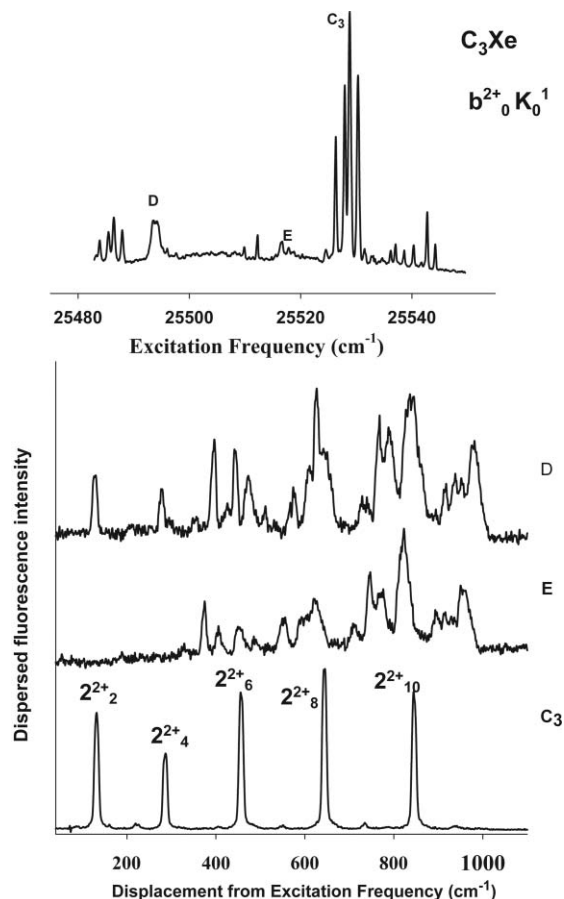

FIG. 7. Top trace: Excitation spectrum of C_3Xe (bands D and E) and C_3 (labeled R(0)+Q(2)) near the 2^{2+}_0 band of free C_3. Wavelength-resolved emission spectra shown in the lower traces were obtained by exciting C_3 and the Xe complex at the labeled frequencies, respectively.

therefore prefer to attribute the diffuseness to spectral congestion.

Figure 6 shows that the emission spectra from the C_3–Xe bands near the 2^{2-}_0 band of C_3 are surprisingly simple: only even quanta of the C_3-bending vibration were observed. These spectra resemble that of free C_3, barring a Franck–Condon node at the second member of the progression, and suggest that the observed level structure of the ground-state complex is that of a linear molecule. The observed progression can thus be assigned as $\upsilon_4'' = 2n$, $n = 2$–5, where $\nu_4(\pi)$ is the C_3 bending vibration. It is found that the levels of $\upsilon_4'' = 2$, 4, and 6 are shifted to higher frequency compared to those of free C_3, in contrast to what is found in the Ar- and Kr-complexes. This implies that the Xe atom bonds more weakly to C_3 in its bending-excited levels than to C_3 in its zero-point level; the binding strengths of the $\upsilon_4'' \geq 2$ levels increase progressively as υ_4'' increases, and eventually those of $\upsilon_4'' \geq 8$ become larger than that of $\upsilon_4'' = 0$.

The observed C_3-bending vibrational levels of the C_3–Ar,[10] C_3–Kr, and C_3–Xe complexes are plotted in Fig. 8 along with those of free C_3.[15,27] The Ar- and Kr-complexes both show the same trends: as the bending quantum number increases, the C_3-bending frequencies (level spacings) of these two complexes are progressively red-shifted relative to those of free C_3. The magnitude of the red-shift is roughly proportional to the polarizabilities of the Ar and Kr atoms, as

discussed in Sec. IV. The level structure of the Xe complex is not easily understood. The first few levels are shifted to higher energy than those than free C_3; above $\upsilon_4'' = 4$ the energy level spacing becomes more regular, reaching a value of about 169 cm^{-1} ($2\nu_4$). More discussion of the vibrational
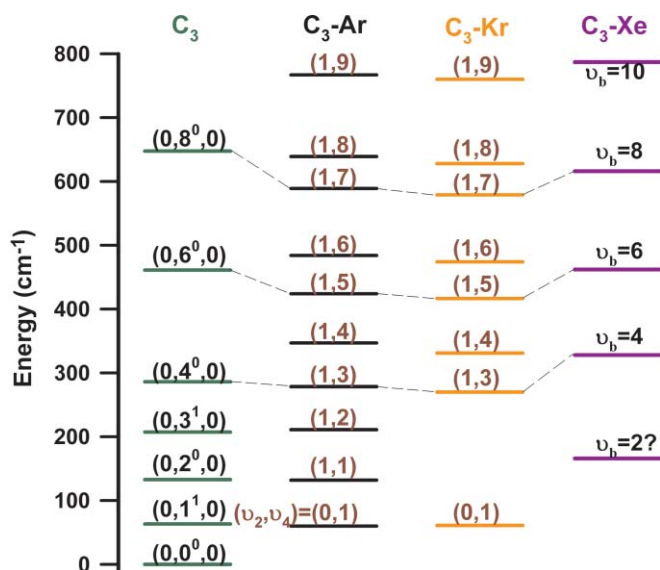
FIG. 8. The C_3-bending levels of free C_3, C_3–Ar, C_3–Kr, and C_3–Xe.

TABLE IV. The energies and vibrational assignments of the lower levels observed from the emission from seven C$_3$–Xe upper levels at 25 004.7,[a] 25 015,[b] 25 026.6,[c] 25 406.6, 25 430.9, 25 494.1,[d] and 25 516.7[e] cm^{-1}.

Vibrational assignment[f]	$v_4' = 2^-$			$v_4' = 4^-$		$v_4' = 2^+$	
	25 004.7	25 015	25 026.6	25 406.6	25 430.9	25 494.1	25 516.7
b$_2$					127		128
b$_2$3$_1$(or 4$_2$)	168				172		
b$_2$3$_1$5$_2$(or 4$_2$5$_2$)						188(vw)[g]	
b$_2$3$_1$5$_3$(or 4$_2$5$_3$)					200(w)[g]		
b$_4$?	254		257(w)				
b$_4$5$_2$?							278
?					283(vw)		
b$_4$3$_1$?							294(sh)[g]
b$_4$3$_1$5$_2$?				316	312		
4$_4$	329					328(vw)	
4$_4$5$_1$	340(sh)	340			337		
4$_4$5$_2$			349		347		
4$_4$5$_3$							354
4$_4$5$_4$			366	363			
4$_4$3$_1$				370(sh)			
4$_4$3$_1$5$_1$				377(sh)		374	
4$_4$3$_1$5$_2$					384(b)		
4$_5$					393(b)		396
4$_5$5$_2$					409(vw)	406	
4$_5$5$_4$					426(w)		426
4$_5$5$_6$							443
4$_5$5$_7$					448	451	
4$_6$	462			460		463(sh)	465(sh)
4$_6$5$_1$	475	473					473
4$_6$5$_2$			481				
4$_6$5$_3$					489	486	491
4$_6$3$_1$			504	505			
4$_6$3$_1$5$_1$				515			511
4$_6$3$_1$5$_3$					529(b)[g]		
4$_7$				537	539(b)	542(sh)	
4$_7$5$_1$				548(sh)		552	
4$_7$5$_2$				555(sh)	559(b)		
4$_7$5$_3$					572(sh)		567
4$_7$3$_1$							575
4$_7$3$_1$5$_2$						592(b)	
4$_7$3$_1$5$_4$						605(b)	
4$_7$3$_2$							611
4$_8$	616					614(b)	
4$_8$5$_1$	624(sh)			625		623	627
4$_8$5$_1$?		630			631		635(sh)
4$_8$5$_2$			639				642(sh)
4$_8$5$_3$					648		650(sh)
4$_8$3$_1$				659			657(sh)
4$_8$3$_1$5$_2$				680	683		
4$_8$3$_1$5$_3$					695(sh)		
4$_9$					703(sh)		
4$_9$5$_1$				709	710(sh)	713	
4$_9$5$_2$				724			
4$_9$5$_3$				734			729(b)
4$_9$5$_4$							740(b)
4$_9$3$_1$				746(sh)	747(sh)	747	
4$_9$3$_1$5$_1$				760(sh)	758		
4$_9$3$_1$5$_2$					771(sh)	772	768(b)

TABLE IV. (*Continued.*)

Vibrational assignment[f]	$v_4' = 2^-$			$v_4' = 4^-$		$v_4' = 2^+$	
	25 004.7	25 015	25 026.6	25 406.6	25 430.9	25 494.1	25 516.7
$4_9 3_1 5_3$				778			
4_{10}	785						790(b)
$4_{10} 5_1$							798(sh)
$4_{10} 5_2$		803		805			
$4_{10} 5_3$			810				
$4_{10} 5_4$						823	
$4_{10} 3_1$				829	828		828(sh)
$4_{10} 3_1 5_1$							836(b)
$4_{10} 3_1 5_2$				845			844(b)
$4_{10} 3_1 5_3$					850		
$4_{10} 3_1 5_4$							856(sh)
$4_{10} 3_1 5_5$							861(sh)
4_{11}				866	867		
$4_{11} 5_2$				881			
$4_{11} 5_3$					893	895	
$4_{11} 5_4$				899			
$4_{11} 3_1$					909(sh)		911(sh)
$4_{11} 3_1 5_1$						915	918
$4_{11} 3_1 5_3$						933	
$4_{11} 3_1 5_4$							938
4_{12}						954	951
$4_{12} 5_2$							975(b)
$4_{12} 5_3$							981(b)

[a]Band A of Fig. 6.
[b]Band B of Fig. 6.
[c]Band C of Fig. 6.
[d]Band D of Fig. 7.
[e]Band E of Fig. 7.
[f]v_3: vdW stretch frequency, v_4: C_3-bending frequency, $v5$: vdW bending frequency.
[g]vw; very weak; w: weak; sh: shoulder of a broad feature; b: broad.

frequencies and the geometries of the Xe-complex is given in Secs. VI B and VII.

VI. *AB INITIO* CALCULATIONS OF THE C_3–Xe COMPLEX

A. Geometry and energy calculations

Ab initio calculations of its ground state potential surface have been carried out for the C_3–Xe complex. An effective core potential was chosen to describe the inner $1s$-$3d$ electrons of the Xe atom.[26] The carbon atoms and the outer 26 electrons of the Xe atom were treated with aug-cc-pVTZ basis sets.[24–26] No attempt was made to use larger basis sets, such as pVQZ, because these do not run efficiently on our computer system (64 bits, 32 Gigabytes memory).

The global minimum of the potential surface is found to be a planar slightly distorted Y-shaped complex, (Y), where the structure is ρ(C_3 bond angle) = 170°, r(C–C bond length) = 1.298 Å, and R(vdW bond length, Xe to the center of mass of C_3) = 4.0 Å. There are two equivalent minima, which correspond to the in-plane bending angles $\phi = 240°$ and 300°. (The symmetrical Y-shaped configuration is defined as $\phi = 270°$, so that the Xe atom lies slightly off the "stalk" of the Y.) Another isomer where the C_3 molecule is bent in the

opposite direction ($\uparrow$) lies about 20 cm^{-1} higher. We call this T-shaped, from the direction of the serifs on the printed letter T. (This isomer is defined as having $\phi < 180°$, while the Y-shaped isomer has $\phi > 180°$.) These two isomers will interconvert rapidly, as the C_3 molecule executes its zero-point bending motion.

Isomerization by internal rotation about the inertial c-axis, which is perpendicular to the plane of the Xe complex, is less likely because the minimum energy pathway requires that a barrier of about 150 cm^{-1} be surmounted. A saddle point is found at $\phi = 175° \pm 20°$ or $5° \pm 20°$, R = 5.2–5.4 Å. It corresponds to another isomer which we call the L-isomer, where the Xe atom lies close to one of the terminal carbon atoms along the inertial a-axis of C_3. This isomer lies about 120 cm^{-1} above the Y-isomer.

We have examined the shape of the potential surface at values of ρ corresponding to the classical turning points of the bending vibration of free C_3 for $v = 0, 2, 4,$ and 6. From the bending potential curve of Ref. 19, these turning points occur near $\rho = 142°, 125°, 118°,$ and 112°, respectively. When the C_3 molecule is bent, up to about $\rho = 120°$, no saddle point is found near $\phi \sim 0°$ or 180°. However, when ρ is 118°, an L-isomer of nearly linear shape ($\wedge$—), a local minimum, can be identified near $\phi = 180°$–205° or 335°–360°, with
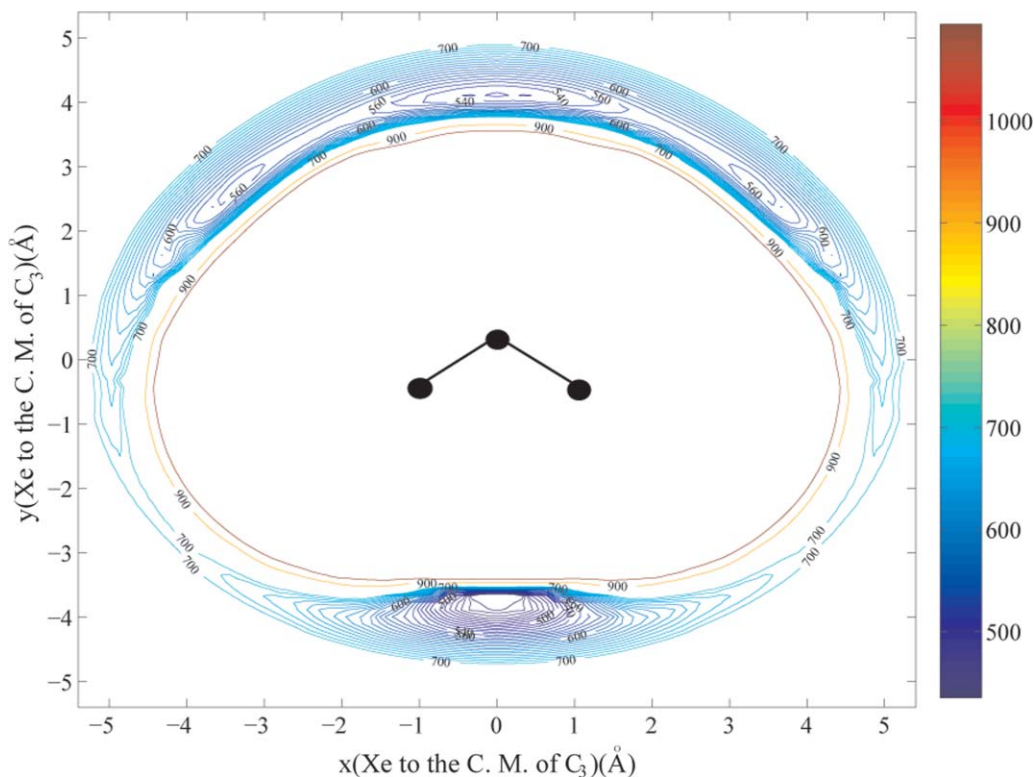
FIG. 9. Contour plot of the CCSD(T) energies of the C$_3$–Xe vdW complex versus the (x,y) coordinates of the Xe atom relative to the center-of-mass of bent C$_3$ (at $\rho = 112°$ and r(C–C) = 1.298 Å). The energies are expressed in units of cm^{-1} relative to the potential minimum of the complex. Contours with energies below 700 cm^{-1} are given for every 10 cm^{-1}. Contours with energy above 700 cm^{-1} (shown only in the repulsive part) are given for every 100 cm^{-1}.

R = 4.8–5.0 Å. If ρ decreases further, the Xe atom bonds even more strongly along the a-axis of the bent C$_3$ molecule; at $\rho = 112°$, the structure corresponds to $\phi = 0°$ or 180° and R = 4.8 Å; the energy of the L-isomer is then ~60 cm^{-1} below that of the Y-isomer for the same C$_3$-bending excitation. Cuts through the potential surface of the Xe-complex at $\rho = 112°$ are illustrated in Figs. 9–11.

Figure 9 is a contour plot of the CCSD(T) energies of the Xe complex at $\rho = 112°$ in the range R = 3.6–5.4 Å. The instantaneous position of the Xe atom relative to the center-of-mass (C.M.) of the C$_3$ molecule is expressed in Cartesian coordinates. The energies in Fig. 9 are relative to the global minimum of the ground electronic state of the Xe complex. The Y-shaped isomer is less stable than the T-shaped isomer at short vdW bond lengths, but this energy order reverses when R is greater than 4.4 Å. At this point, the complex can undergo a fairly large amplitude vdW bending motion from Y-shape to near L-shape. If R is shorter than 4.8 Å, a fairly large barrier prevents the T-to-Y isomerization from occurring unless the C$_3$ molecule bends out of plane. When R is greater than about 5 Å, there is essentially free internal rotation around the c-axis of the Xe-complex, which allows easy interconversion of the three isomers.

It is not easy to see the minima corresponding to the L-isomer in Fig. 9, because the grid of points is not fine enough. Figure 10 is an alternative representation of Fig. 9, showing how the two equivalent potential minima of the Y-isomer move apart as the vdW bond length increases, giving rise to pronounced local minima near the L-configuration at

R = 4.6–4.8 Å. They are marked with arrows in the figure. Large amplitude vdW bending motion would allow adiabatic Y-to-L conversion. Figure 11 shows a contour plot of the CCSD(T) energies at $\rho = 112°$ against the out-of-plane C$_3$-bending angle, θ, and the in-plane vdW bending angle, ϕ, at a fixed vdW bond length, R = 4.8 Å. It confirms that the complex prefers to be planar and that the L-isomer lies at a local minimum (i.e., $\phi \sim 0°$ or 180°), representing a stable isomer when ρ is small (i.e., for strongly bent C$_3$, with large values of υ_{bend}). In contrast, no L-isomer could be located in the potential of the C$_3$–Ar complex.

Figure 9 also shows that, over the complete range $\rho = 112$–180° which we have studied by *ab initio* calculation, the minimum energy pathway to dissociation is via the high vibrational levels of the L-isomer.

B. Vibrational frequencies

Assuming that the rare gas atom perturbs the C$_3$ bending motion only slightly, the C$_3$-bending frequencies of the three possible isomers can be estimated from the CCSD(T) potential calculated at values of ρ corresponding to the classical turning points (see Sec. IV A). The value of R was taken as 3.8 Å. It has been shown that the potential curve of the C$_3$-bending vibration of free C$_3$ is very flat and that it requires a fairly large basis set to reproduce the observed vibrational levels.[19,20] Using a small basis set such as aug-cc-pVTZ, a calculated frequency tends to be higher than the observed values.[19,20] Our observed C$_3$-bending intervals [E(υ_4+2)
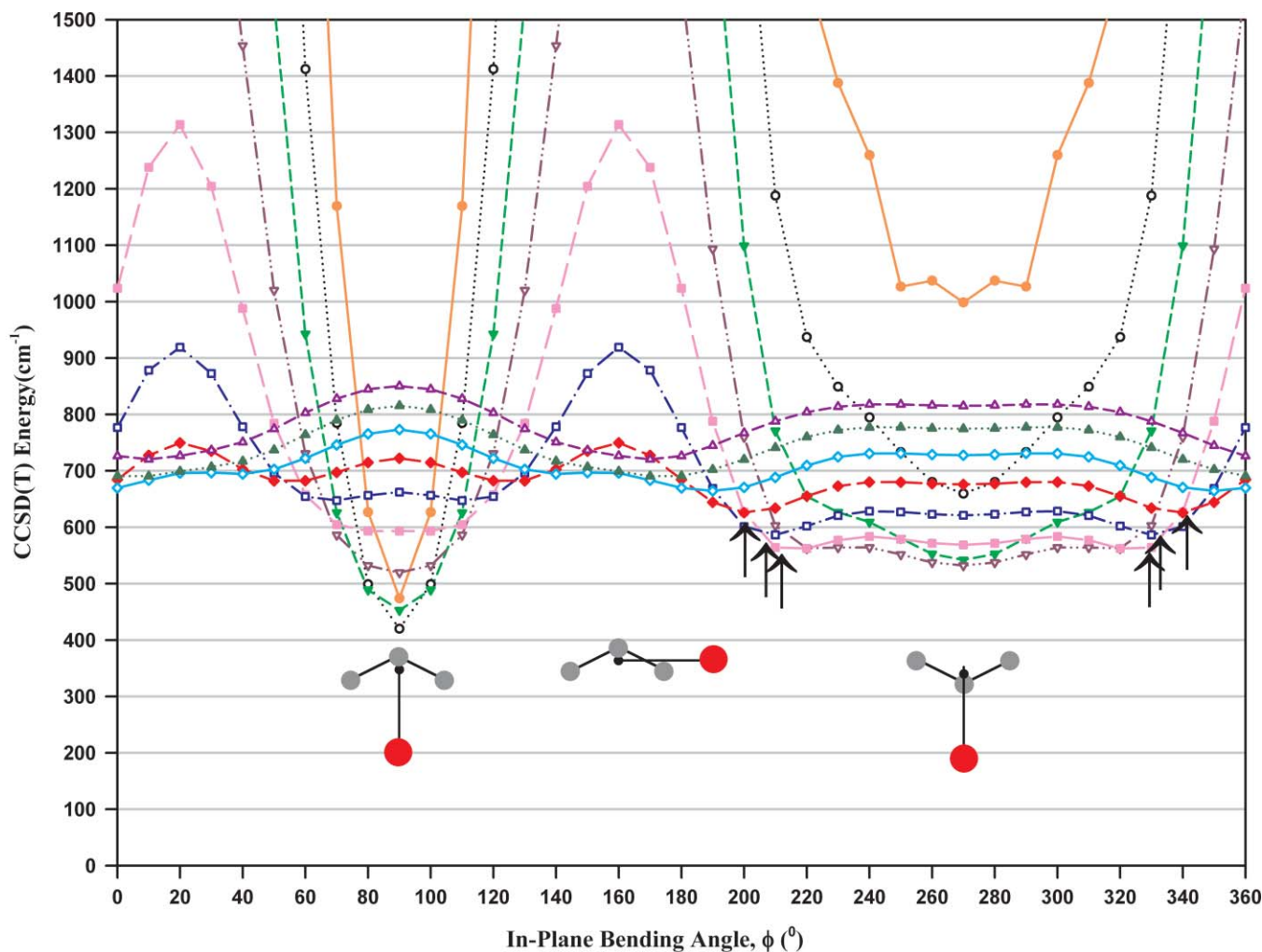
FIG. 10. The CCSD(T) energy curves of the C_3–Xe vdW complex versus the in-plane vdW bending angle, ϕ, for R = 3.6–5.4 Å at $\rho = 112°$ and r(C–C) = 1.298 Å. R (vdW bond length from the Xe atom to the center-of-mass of C_3) = 3.6 Å, —●— 3.8 Å, · ·○· ·; 4.0 Å, - -▼-; 4.2 Å,–· · -▽-· -; 4.4 Å,- - ■ -; 4.6 Å, – · –□–; 4.8 Å,- - ◆-; 5.0 Å, —◆—; 5.2 Å,· · ▲· · ·; 5.4 Å,-- △--. Arrows indicate the minima corresponding to the L-isomer at 4.4, 4.6, and 4.8 Å.

— E(υ_4) = 133, 155, and 169 cm^{-1}] lie slightly below those calculated for the Y- and L-isomers (166 and 186 cm^{-1}, respectively), but above that calculated for the T-isomer (130 cm^{-1}). These results appear to be consistent with our spectral assignment that the vibrationally excited levels ($\upsilon_4 \geq 4$) of C_3–Xe act like those of a linear molecule. Unfortunately, the assignments of the vibrational levels below 329 cm^{-1} (above the zero-point energy level) are subject to uncertainty, since we do not know if they belong to the linear or the T-isomer. This can be seen in Table IV, which lists all the observed energy levels and our tentative assignments of the Xe complex from our wavelength-resolved emission spectra.

The vdW stretching frequency of the C_3–Xe complex has been estimated as in Sec. IV for the C_3–Kr complex. The resulting estimates for the T-, Y- and L-isomers are 50, 40, and 37 cm^{-1} for $\upsilon_4 \geq 4$. From our calculation, the anharmonicity constants, x_{ii}, of the three isomers are the same to within 0.2 cm^{-1}, being in the range -1.0 to -1.2 cm^{-1}. When the C_3 molecule is nearly linear, the properties of the T- and Y-isomers become almost the same, and the vdW stretching frequency of the Y-isomer approaches the value of 50 cm^{-1}. Since the observed vibrational levels of the Xe complex from our emission spectra are high vibrational levels, the structure should be more like the Y-isomer. Hence the observed vdW stretching frequency should be about 40 cm^{-1}.

Figure 11 shows that the potential surface is almost flat in the region from $\phi = 220°$ to $320°$, when R is greater than about 4.6 Å. The vdW bending frequency is therefore expected to become smaller when $\upsilon_4 \geq 4$. Two low frequencies, 7–10 and 12–18 cm^{-1} have been identified, as shown in Table IV. The latter seems to be twice the former. Since higher levels of the C_3–Xe complex with $\upsilon_4 \geq 4$ appear to behave like those of a linear molecule, the two vdW bending motions can be treated as a degenerate vibration (ν_5) with π symmetry. We therefore expect to observe progressions in even quanta of ν_5 in the emission spectra. Hence we assign the low frequency, 7–10 cm^{-1}, as the ground state vdW bending frequency of the complex.

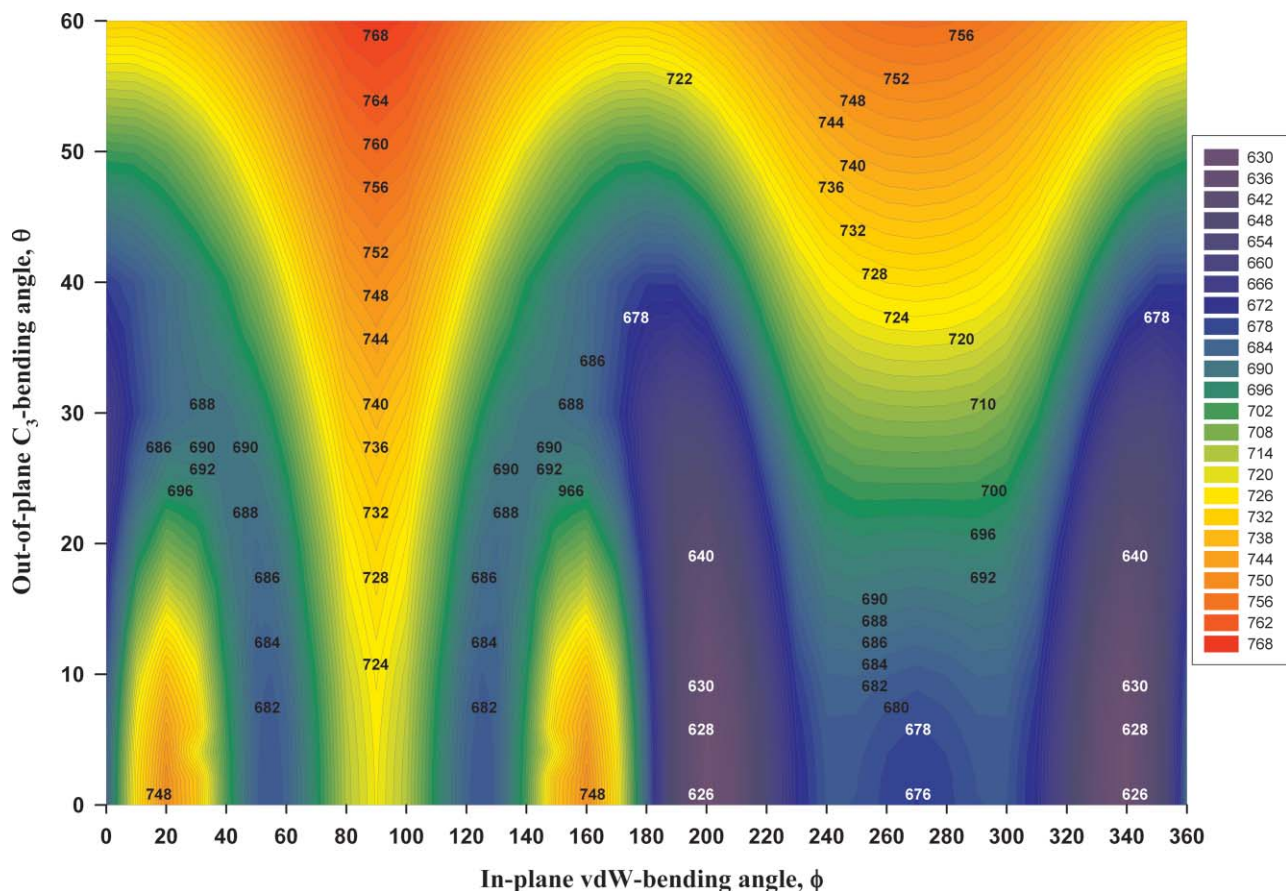The emission spectrum from the vdW band of C_3–Xe at 25 015.5 cm^{-1} shows mostly transitions to the odd-numbered

FIG. 11. Contour plot of the calculated CCSD(T) energy of the C₃–Xe complex versus out-of-plane C₃-bending angle, θ, and in-plane vdW bending angle, ϕ, at $\rho = 112°$ and fixed vdW bond length, R = 4.8Å. Contours are given for every 2 cm^{-1} from 626 to 676 cm^{-1}; for energies above 680 cm^{-1}, contours are shown for every 5 cm^{-1}.

levels of υ_5'', which are forbidden transitions. This may explain the weakness of the LIF spectrum. Instead, two other nearby bands at 25 004.7 and 25 026.6 cm^{-1} have emission down to the even-numbered levels of υ_5''. On the other hand the levels at 25 406.6, 25 430.9 and 25 516.7 cm^{-1} emit to the odd- and even-numbered levels of both υ_4'' and υ_5''. Since the Xe-complex appears to behave as a linear molecule in the $\tilde{A}$ state and in the levels of the $\tilde{X}$ state with $\upsilon_4 \geq 4$, transitions are only expected to even quanta of υ_4 or υ_5 in the absence of vibronic coupling. Extensive υ_5''-progressions were also observed in the emission spectra from the vdW bands with $\upsilon_4' = 2^+$ and 4^-. Hence, as for the $\tilde{A}$ state, various frequency intervals in the range of 10.3–12.0 cm^{-1} appearing in the excitation spectra of the Xe-complex are assigned as single quanta of the vdW bending vibration of the $\tilde{A}$ state.

VII. DISCUSSION

Although some LIF spectra of the C₃–Kr complex have been recorded at higher resolution, ∼0.06 cm^{-1}, this is unfortunately not sufficient to resolve the rotational structure. Since the experimental conditions used to generate the Ar, Kr, and Xe complexes are very similar and the Ar complex is known

to be a 1:1 complex,[10] we presume that the Kr and Xe complexes observed in this work are also 1:1 complexes.

No direct experimental information about the geometries of the Kr and Xe complexes at equilibrium is available yet, but we assume that they are also T-shaped, like the Ar complex, for which the structure was determined from our previous higher resolution LIF spectra.[10] The wavelength-resolved emission spectra and the LIF excitation spectra of the Kr complex show considerable resemblance to those of the Ar complex, which leads us to believe that the Kr complex is T-shaped in both its $\tilde{X}$ and $\tilde{A}$ states; this is consistent with our *ab initio* calculation of its ground electronic state structure.

The *ab initio* calculations of the Xe complex showed that the T-/Y-shape will be its equilibrium structure, but at υ_b (or υ_4) ≥ 4, an L-isomer becomes increasingly stable. Examination of the MOs calculated by the Hartree–Fock self-consistent field method indicates that the L-isomer of the Xe complex is stabilized by the mixing of some π^* or σ^* character into the $1\pi_u$ orbital. The $\tilde{A}\,^1\Pi_u$ state, lying at 24 675.6 cm^{-1},[12,13,16] is known to have the configuration $\ldots(2\sigma_u)^1(1\pi_u)^4(1\pi_g)^1$,[28–30] while the $\tilde{B}\,^1\Sigma_u^-$ and $\tilde{B}'\,^1\Delta_u$ states from the configuration $\ldots(2\sigma_u)^2(1\pi_u)^3(1\pi_g)^1$ lie at about 29 500 cm^{-1}.[28–30] The $\tilde{B}$ and $\tilde{B}'$ states are predicted to cross the $\tilde{A}$ state at an elongated C–C bond length, ∼1.42 Å. Hence, it is very likely that the $\tilde{A}$ state of the Xe complex has

only a small potential barrier between the T- and L-shapes to account for the quick conversion from T to L within the fluorescence lifetime ($\sim$200 ns) of the $\tilde{A}$ state. This could perhaps have been anticipated because the electron distributions in the $\tilde{A}$, $\tilde{B}$, and $\tilde{B}'$ excited electronic states stabilize the L-shaped Xe complex. It could also be tested by examining the excitation spectra of the Xe complex near higher vibrational levels of the $\tilde{A}$ state. The vibrational assignments of the high vibrational levels of the $\tilde{A}$ state of C_3, and a search for the $\tilde{B}$ and $\tilde{B}'$ states, are in progress in our laboratory.[31] It is hoped that we can address this question in the near future.

The emission spectra from the 2^{4-} and 2^{2+} levels of $C_3(\tilde{A})$ down to the bending levels with $E_{vib} \leq 1000$ cm^{-1} were found to be very similar to each other,[10] as might be predicted from the strong mixing caused by the orbital angular momentum.[17] For the C_3–Ar complex it was found[10] that the vdW levels near the energy of the C_3, 2^{2+} level emit more strongly to even υ_b levels of the ground electronic state than to odd ones; however, contrary results were observed from those near the C_3, 2^{4-} level. Similar patterns are found for the Kr and Xe complexes, as can be seen in Tables II and III. These results indicate that the Rg atom has a non-negligible effect on the orbital angular momentum of the $\tilde{A}$ state.

The binding energies of the Kr and Xe complexes are estimated to be 280 and 300 cm^{-1}, respectively, from CCSD(T)/aug-cc-pVTZ calculations at their equilibrium geometries. The calculations also predict that the binding energy of the T-isomer increases as the C_3 bending quantum number increases. The magnitudes of the red-shifts from the free C_3 transitions, listed in Table I, allow us to estimate that the binding energies of the $\tilde{A}$ states of these two complexes lie in the ranges 302–318 and 334–336 cm^{-1}.

VIII. CONCLUSIONS

Bands of the $\tilde{A}$–$\tilde{X}$ electronic transitions of the C_3–Kr and C_3–Xe complexes have been discovered accompanying bands of the $\tilde{A}$–$\tilde{X}$ system of the free C_3 molecule, though not the (0,0) band itself. No predissociations were detected in the $\tilde{A}$ states of the Kr and Xe complexes. Our experimental observations lead to the conclusion that both the upper and lower electronic states of the Kr complex are T-shaped. The C_3-bending vibrational levels of the Kr complex are lower in energy than those of free C_3 because of dipole-induced dipole interaction between the Kr atom and C_3 in its higher bending levels. The energy lowerings observed for the Kr complex are larger than those found for the Ar complex, reflecting the larger polarizability of Kr. A simple perturbed harmonic oscillator model based on dipole-induced dipole interaction roughly reproduces the C_3-bending vibrational levels of the Kr complex, with the interaction potential taken as $V_2 \cos 2\theta$, where $V_2 = 6.3$ cm^{-1}.

Neglecting the large amplitude motion and anharmonicities, the vibrational frequencies of the ground electronic state of C_3–Kr were determined to be $\nu_2 = 111(7)$, ν_3(vdW stretch) $= 37(2)$, $\nu_4 = 40(3)$, and ν_6(vdW bend) $= 8(2)$ cm^{-1}.

Emission spectra from the $\tilde{A}$, b^{2-} levels of the C_3–Xe complex give evidence that a linear isomer of the complex becomes observable when four or more quanta of the C_3 bending vibration are excited. The vibrational frequencies of this L-isomer of the ground electronic state of the Xe complex were found to be ν_3(vdW stretch) $= 42(3)$, ν_4(C_3-bending) $= 76(9)$, and ν_5(vdW bend) $= 8.5(15)$ cm^{-1}.

[1] G. D. Hayman, J. Hodge, B. J. Howard, J. S. Muenter, and T. R. Dyke, J. Mol. Spectrosc. **133**, 423 (1989).
[2] K. A. Walker, T. Ogata, W. Jäger, and M. C. L. Gerry, J. Chem. Phys. **106**, 7519 (1997).
[3] R. J. Le Roy and J. M. Hutson, J. Chem. Phys. **86**, 837 (1987).
[4] Q. Wen and W. Jäger, J. Chem. Phys. **124**, 014301 (2006).
[5] K. J. Higgins and W. Klemperer, J. Chem. Phys. **122**, 244309 (2005).
[6] M. L. Burke and W. Klemperer, J. Chem. Phys. **98**, 1797 (1993).
[7] A. E. S. Miller, C.-C. Chuang, H. C. Fu, K. J. Higgins, and W. Klemperer, J. Chem. Phys. **111**, 7844 (1999).
[8] J. Cabrera, C. R. Bieler, N. McKinney, W. E. van der Veer, J. M. Pio, K. Janda, and O. Roncero, J. Chem. Phys. **127**, 164309 (2007).
[9] J. M. Pio, W. E. van der Veer, C. R. Bieler, and K. C. Janda, J. Chem. Phys. **128**, 134311 (2008).
[10] G. Zhang, B.-G. Lin, S.-M. Wen, and Y.-C. Hsu, J. Chem. Phys. **120**, 3189 (2004).
[11] F. M. Phelps III, *M. I. T. Wavelength Tables* (MIT, Cambridge, MA, 1982).
[12] L. Gausset, G. Herzberg, A. Lagerqvist, and B. Rosen, Astrophys. J. **142**, 45 (1965).
[13] W. J. Balfour, J. Cao, C. V. V. Prasad, and C. X. W. Qian, J. Chem. Phys. **101**, 10343 (1994).
[14] D. W. Tokaryk and D. E. Chomiak, J. Chem. Phys. **106**, 7600 (1997).
[15] F. J. Northrup and T. J. Sears, J. Opt. Soc. Am. B **7**, 1924 (1990).
[16] G. Zhang, K.-S. Chen, A. J. Merer, Y.-C. Hsu, W.-J. Chen, S. Shaji, and Y.-A. Liao, J. Chem. Phys. **122**, 244308 (2005).
[17] Ch. Jungen and A. J. Merer, Mol. Phys. **40**, 95 (1980).
[18] J. M. Chao, M. Sc. thesis, National Taiwan University, (2003).
[19] P. Jensen, C. M. Rohlfing, and J. Almlöf, J. Chem. Phys. **97**, 3399 (1992).
[20] M. Mladenović, S. Schmatz, and P. Botschwina, J. Chem. Phys. **101**, 5891 (1994).
[21] R. H. Orcutt and R. H. Cole, J. Chem. Phys. **46**, 697 (1967).
[22] A. D. Buckingham, Adv. Chem. Phys. **12**, 107 (1967).
[23] Gaussian 2003, revision D.02, M. J. Frisch, G. W. Trucks, H. B. Schlegel *et al.*, Gaussian, Inc., Pittsburgh, PA, 2003.
[24] T. H., Dunning, Jr., J. Chem. Phys. **90**, 1007 (1989).
[25] R. A. Kendall, T. H., Dunning, Jr., and R. J. Harrison, J. Chem. Phys. **96**, 6796 (1992).
[26] K. A. Peterson, D. Figgen, E. Goll, H. Stoll, and M. Dolg, J. Chem. Phys. **119**, 11113 (2003).
[27] C. A. Schmuttenmaer, R. C. Cohen, N. Pugliano, J. R. Heath, A. L. Cooksy, K. L. Busarow, and R. J. Saykally, Science **249**, 897 (1990).
[28] J. Kalcher and R. Janoschek, J. Mol. Struct. **234**, 509 (1991).
[29] K. Ahmed, G. G. Balint-Kurti, and C. M. Western, J. Chem. Phys. **121**, 10041 (2004).
[30] S. Saha and C. M. Western, J. Chem. Phys. **125**, 224307 (2006).
[31] C.-W. Chen, A. J. Merer, J.-M. Chao, and Y.-C. Hsu, J. Mol. Spectrosc. **263**, 56 (2010).